

## A positive period derivative in the quasi-periodic eruptions of ZTF19acnskyy

JOHEEN CHAKRABORTY , <sup>1,\*</sup> SAUL A. RAPPAPORT , RICCARDO ARCODIA , <sup>1,2</sup> ITAI LINIAL , <sup>3,4,†</sup>  
 GIOVANNI MINIUTTI , <sup>5</sup> KEVIN B. BURDGE , JORGE CUADRA , <sup>6,7</sup> MARGHERITA GIUSTINI , <sup>5</sup>  
 LORENA HERNÁNDEZ-GARCÍA , <sup>8,9</sup> ERIN KARA , PAULA SÁNCHEZ-SÁEZ , <sup>10</sup> AND PHILIPPE YAO 

<sup>1</sup>Department of Physics & Kavli Institute for Astrophysics and Space Research, Massachusetts Institute of Technology, Cambridge, MA 02139, USA

<sup>2</sup>Black Hole Initiative at Harvard University, 20 Garden Street, Cambridge, MA 02138, USA

<sup>3</sup>Department of Physics & Columbia Astrophysics Laboratory, Columbia University, New York, NY 10027, USA

<sup>4</sup>Center for Cosmology and Particle Physics, Physics Department, New York University, New York, NY 10003, USA

<sup>5</sup>Centro de Astrobiología (CAB), CSIC-INTA, Camino Bajo del Castillo s/n, 28692 Villanueva de la Cañada, Madrid, Spain

<sup>6</sup>Departamento de Ciencias, Facultad de Artes Liberales, Universidad Adolfo Ibáñez, Av. Padre Hurtado 750, Viña del Mar, Chile

<sup>7</sup>Millennium Nucleus on Transversal Research and Technology to Explore Supermassive Black Holes (TITANS), Gran Bretaña 1111, Playa Ancha, Valparaíso, Chile

<sup>8</sup>Instituto de Estudios Astrofísicos, Facultad de Ingeniería y Ciencias, Universidad Diego Portales, Av. Ejército Libertador 441, Santiago, Chile

<sup>9</sup>Centro Interdisciplinario de Data Science, Facultad de Ingeniería y Ciencias, Universidad Diego Portales, Av. Ejército Libertador 441, Santiago, Chile

<sup>10</sup>European Southern Observatory, Karl-Schwarzschild-Strasse 2, 85748 Garching bei München, Germany

<sup>11</sup>Department of Astrophysical Sciences, Princeton University, Princeton, NJ 08544, USA

### ABSTRACT

We report the first direct measurement of the period derivative in a quasi-periodic eruption (QPE), finding a smoothly *increasing* period with  $\dot{P} \approx (1.7 \pm 0.02) \times 10^{-2} \text{ d d}^{-1}$  in the source ZTF19acnskyy/“Anskey”. Most models for QPEs invoke repeated interactions of a stellar-mass orbiting companion around the supermassive black hole (SMBH) in an extreme mass-ratio inspiral (EMRI). In these scenarios, a positive  $\dot{P}$  is surprising, but not impossible to produce. We explore several possible explanations for the observed  $\dot{P}$ , including stable mass-transfer driven by impulsive mass loss events in an EMRI, velocity kicks at pericenter due to tidal interactions with the SMBH, apparent period changes due either to general relativistic precession effects in an EMRI or light travel-time delays in a hierarchical SMBH binary, and mass-transfer variations in a thermal/viscous disk instability model. We find that none of the considered models provides a complete explanation for the data, motivating further work on physical explanations for positive period derivatives in QPEs.

**Keywords:** Supermassive black holes (1663); X-ray astronomy (1810); Transient sources (1851)

### 1. INTRODUCTION

Quasi-periodic eruptions (QPEs) are recurring soft X-ray transients from the supermassive black holes (SMBHs) in some nearby galaxy nuclei (Miniutti et al. 2019; Giustini et al. 2020; Arcodia et al. 2021, 2024, 2025; Chakraborty et al. 2021, 2025a; Quintin et al. 2023; Nicholl et al. 2024; Hernández-García et al. 2025a; Baldini et al. 2026). They show peak luminosities ranging from  $L_{\text{peak}} \sim 10^{42-44} \text{ erg s}^{-1}$ , recurrence times

of  $T_{\text{rec}} \sim 2.5 - 300 \text{ hr}$ , blackbody-like spectra with temperatures of  $kT \sim 50 - 250 \text{ eV}$ , SMBH masses of  $\sim 10^{5-7.5} M_{\odot}$ , and host galaxy redshifts up to  $z \lesssim 0.1$ . In some sources, QPEs have emerged months to years after Tidal Disruption Events (TDEs) selected by X-ray (Miniutti et al. 2023; Chakraborty et al. 2021; Baldini et al. 2026) and optical surveys (Quintin et al. 2023; Nicholl et al. 2024; Chakraborty et al. 2025a), providing an interesting theoretical puzzle as well as a promising avenue for future discoveries.

The leading model class thus far explains the recurring X-ray bursts via repeated interactions with a gravitationally captured stellar-mass object around the SMBH

\* joheen@mit.edu

† NASA Einstein Fellow

in an extreme mass-ratio inspiral (EMRI; e.g. King 2020; Xian et al. 2021; Suková et al. 2021; Krolik & Linial 2022; Linial & Sari 2023; Lu & Quataert 2023; Franchini et al. 2023; Linial & Metzger 2023; Tagawa & Haiman 2023; Yao et al. 2025)—though we will soon see the more appropriate term in our case may be extreme mass-ratio *outspiral*. In this picture, the bursts may arise from collisions of the orbiting companion with the accretion disk surrounding the SMBH (perhaps initially formed by the precursor TDE), or by repeated mass-loss of the companion near pericenter. EMRI models have provided an attractive framework to interpret the zeroth-order observational properties of QPEs, such as their amplitudes, quasi-periodicity, rates, and spectra. Still, there remain multiple open questions related to e.g. the precise source of short- and long-term timing variations observed in some QPEs (Miniutti et al. 2025; Arcodia et al. in prep.) and the burst energetics across the population (Mummery 2025; Linial et al. 2025). Alternative models of accretion disk instabilities driven by e.g. nodal precession (Raj & Nixon 2021; Middleton et al. 2025) or variations in magnetic viscosity (Śniegowska et al. 2020, 2023; Pan et al. 2022, 2023, 2025; Kaur et al. 2023) are thus worthwhile avenues for ongoing investigation. It is entirely possible that the growing family of QPEs may arise from a combination of different physical mechanisms.

The most extreme known source of QPEs is the nuclear transient ZTF19acnskyy/“Anskey” (Sánchez-Sáez et al. 2024), which hosts long, luminous eruptions of integrated energy budget  $L\Delta t \gtrsim 100\times$  larger and recurrence time  $\gtrsim 10\times$  longer than typical QPE sources (Hernández-García et al. 2025a). The eruptions also uniquely show broad, time-evolving absorption lines potentially indicating relativistic outflows powering the QPEs (Chakraborty et al. 2025b). The optical/UV transient nature of Anskey is uncertain, with possible interpretations including an AGN turn-on around a  $\sim 10^6 M_\odot$  SMBH or a featureless TDE (Sánchez-Sáez et al. 2024; Zhu et al. 2025). Furthermore, Hernández-García et al. (2025b) recently reported a *doubled* recurrence time and burst duration between 2024-2025, followed by a steady increase of  $\sim 0.1$  d per flare. Anskey’s extraordinary characteristics provide a stress-test for the very limits of any physical model of QPEs.

In this paper, we present data from our continued X-ray monitoring campaign throughout 2025-2026. In total, we observed 23 bursts—of which 19 were consecutive, the most in any source thus far—which enable a unique timing analysis sensitive to secular period evolution. We outline the observations and data reduction procedures in Section 2 and present the key results of

**Table 1.** Observed peak times and luminosities throughout 2025-2026. Measurement errors are added in quadrature with a systematic model timing uncertainty of 0.1 d.

Epoch	MJD	$\sigma_-$ (days)	$\sigma_+$ (days)	$L_{\text{peak}}$ ( $10^{43}$ erg s $^{-1}$ )
-2	60690.63	0.10	0.10	$4.2^{+0.5}_{-0.5}$
0	60709.36	0.10	0.10	$3.6^{+0.4}_{-0.4}$
1	60719.23	0.10	0.10	$4.3^{+0.5}_{-0.5}$
2	60729.32	0.10	0.10	$4.2^{+0.4}_{-0.4}$
3	60739.35	0.10	0.10	$5.7^{+0.6}_{-0.6}$
4	60749.94	0.10	0.10	$6.0^{+0.6}_{-0.6}$
5	60760.46	0.10	0.10	$5.3^{+0.5}_{-0.5}$
6	60770.71	0.10	0.10	$4.6^{+0.5}_{-0.5}$
7	60781.00	0.10	0.10	$4.6^{+0.5}_{-0.5}$
8	60791.46	0.10	0.10	$4.6^{+0.5}_{-0.5}$
9	60802.32	0.10	0.10	$4.2^{+0.4}_{-0.4}$
10	60813.09	0.10	0.10	$4.8^{+0.5}_{-0.5}$
11	60824.27	0.10	0.10	$4.5^{+0.5}_{-0.5}$
12	60835.38	0.11	0.11	$3.2^{+0.4}_{-0.4}$
13	60846.83	0.17	0.24	$3.8^{+1.6}_{-1.6}$
14	60857.78	0.14	0.12	$3.1^{+1.1}_{-0.7}$
15	60869.51	0.10	0.10	$2.8^{+0.3}_{-0.3}$
16	60881.64	0.10	0.10	$2.6^{+0.3}_{-0.3}$
17	60894.43	0.11	0.11	$2.3^{+0.3}_{-0.3}$
18	60906.71	0.12	0.13	$2.5^{+0.3}_{-0.4}$
27	61024.83	1.08	0.10	$2.2^{+1.3}_{-0.7}$
28	61038.33	0.14	0.13	$2.1^{+0.5}_{-0.5}$
30	61067.48	0.22	0.19	$2.0^{+1.1}_{-0.8}$

our timing analysis in Section 3. We consider several models for the increasing period, and discuss their implications for the long-term fate of the QPEs in Anskey, in Section 4. We make concluding remarks in Section 5.

## 2. OBSERVATIONS AND METHODS

The *NICER* X-ray Timing Instrument (Gendreau et al. 2016) aboard the International Space Station subsequently observed Anskey for a total of 282.5 ks across 263 observations from Jan 05-Jun 16, 2025. We followed the time-resolved spectroscopy approach for light curve estimation outlined in Section 2.1 of Chakraborty et al. (2024a). Spectral fitting and background estimation were performed with the SCORPEON model over a broadband energy range (0.25–10 keV) for data taken in orbit night, and a restricted range (0.38–10 keV) during orbit day. We grouped our spectra with the optimal binning scheme of Kaastra & Bleeker (2016) (`groupstype=optmin` with `groupscale=10` in the

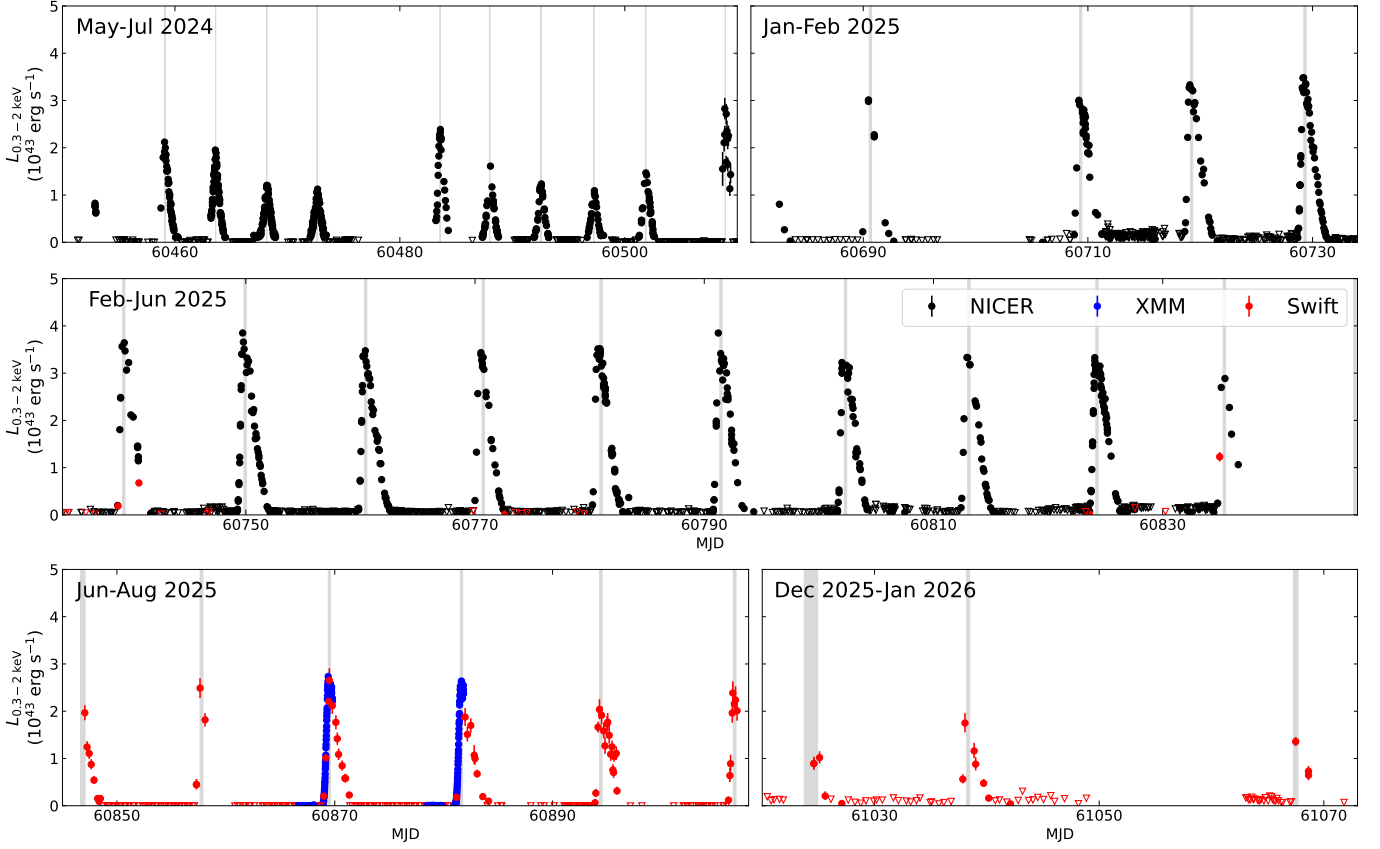


**Figure 1.** The soft X-ray light curve of Ansley from 2024-2026. Data were taken with the *NICER* (black), *Swift* (red), and *XMM-Newton* (blue) observatories. Gray shaded regions correspond to the  $\pm 1\sigma$  contours of  $t_{\text{peak}}$  measurements from our timing model (Table 1).

`ftgrouppha` command) and performed all spectral fitting with the Cash statistic (Cash 1979).

*Swift* X-ray telescope (XRT) data were obtained from the online interface (<https://www.swift.ac.uk/LSXPS>) to the Living *Swift* XRT Point Source (LSXPS) Catalogue (Evans et al. 2023). LSXPS is an automatically updated repository of all *Swift* XRT observations of  $> 100$  second duration in Photon Counting (PC) mode. LSXPS reports X-ray fluxes in counts per second (cps); we converted to cgs units using a conversion factor of  $1 \text{ cps} = 2.2 \times 10^{-11} \text{ erg cm}^{-2} \text{ s}^{-1}$ , which was computed for a 100 eV blackbody spectrum and Galactic neutral absorption with  $N_{\text{H}} = 2.6 \times 10^{20} \text{ cm}^{-2}$ .

*XMM-Newton* data were obtained through GO 096454 in AO 24 (PI: Chakraborty). The observations were taken on July 10/12/22/24, 2025 (OBSIDs 0964540101-0964540401), with the first and third observing quiescence and the second and fourth observing the rise-to-peak of two consecutive eruptions. The *XMM* data provide a deep view into the short-timescale X-ray spectral-timing variability, and will be the subject of forthcoming

work. The data were reduced using *XMM* SASv21.0.0 and HEASoft v6.33. Source products were extracted from a circular region of  $33''$  radius, while the background was extracted from source-free circular region falling on the same detector with a  $60''$  radius. We retained events with  $\text{PATTERN} \leq 4$  (single and double events only) and discarded time intervals with a  $10\text{--}12$  keV count rate  $\geq 1 \text{ counts s}^{-1}$ . Light curves were extracted with `evselect`, corrected for detector efficiency, vignetting, PSF, and bad pixels using `epiclccorr`, and binned to 1 ks in the 0.3-2 keV band.

### 3. RESULTS

In Fig. 1 we show the full light curve of the QPEs in Ansley. To estimate the peak timings, we fit each eruption with a four-parameter exponential rise-and-decay model introduced for QPEs in Arcodia et al. 2022:

$$L(t) = \begin{cases} L_{\text{peak}} \lambda e^{\tau_1 / (t_{\text{peak}} - t_{\text{as}} - t)} & \text{if } t \leq t_{\text{peak}} \\ L_{\text{peak}} e^{-(t - t_{\text{peak}}) / \tau_2} & \text{if } t > t_{\text{peak}} \end{cases}$$

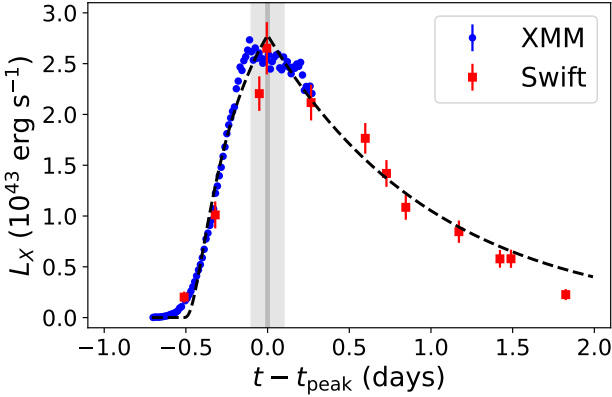


**Figure 2.** Example burst profile from an *XMM*-observed burst (Epoch 15,  $t_{\text{peak}} = 60869.51$ ). The dark gray band shows the model  $t_{\text{peak}}$  error estimated via MCMC. The light gray band shows our additional 0.1 day systematic uncertainty, which accounts for the scatter in *XMM* and *Swift* data near the peak.

where  $L_{\text{peak}}$  is the flare amplitude,  $t_{\text{peak}}$  is the peak timing, and  $\tau_1/\tau_2$  are the rise/decay  $e$ -folding times.  $\lambda \equiv \exp(\sqrt{\tau_1/\tau_2})$  and  $t_{\text{as}} \equiv \sqrt{\tau_1\tau_2}$  are derived parameters setting the normalization and asymptote time; for more discussion, see Arcodia et al. (2022) or Chakraborty et al. (2024a). Uncertainties on  $t_{\text{peak}}$  were initially estimated via MCMC, resulting in characteristic errors of  $\sim 0.01$  d. However, in several cases we found the best-fit model was not a perfect description of the data, and that the model  $t_{\text{peak}}$  disagreed with the measured peak flux by up to  $\lesssim 0.1$  days (see Fig. 2 for an illustrative example of the burst with highest-cadence coverage); as a result, we added in quadrature a 0.1 d uncertainty to all MCMC error estimates to capture the intrinsic model inaccuracy in describing the peak timings. We verified that the choice of  $\sigma_{\text{sys}} \in \{0.05, 0.1, 0.15, 0.2\}$  d does not qualitatively alter our results. The model peak times and luminosities are reported in Table 1.

The bursts reach  $L_{\text{peak}} \approx (2 - 6) \times 10^{43}$  erg s $^{-1}$ , corresponding to time-integrated energy outputs  $L\Delta t \approx (1 - 5) \times 10^{48}$  erg. Assuming radiative efficiencies in the range  $\eta \sim 0.01 - 1$  (e.g. Linial et al. 2025), we find characteristic mass budgets of  $\Delta M_* \sim L\Delta t/(\eta c^2) \sim 10^{-6} - 10^{-4} M_\odot$ . Given that  $\mathcal{O}(100)$  bursts are expected to have occurred thus far—including those observed in 2024 and 2026, and interpolating between observational gaps—we may infer a total mass budget on the order of  $\sim 10^{-4} - 10^{-2} M_\odot$  to date. In other words, the observed QPE properties and lifetime remain consistent with being powered by a stellar-mass object.

In Fig. 3 we show an  $O - C$  (observed minus calculated) diagram of the 2025 QPEs, where  $O$  are the ob-

served peak arrival times (Table 1) and  $C$  are the calculated timings assuming a fixed period, i.e.  $C = T_0 + nP_0$  at  $n$  epochs after a reference timing  $T_0$  for a trial period  $P_0$ . The dominant feature visible in the  $O - C$  diagram is a concave-up trend over the  $\sim 30$  observed epochs. We consider four possible models to describe the timings:

$$T_{M,1} = T_0 + \Delta P_0 n + \frac{1}{2} P_0 \dot{P} n^2 + \dots \quad (1)$$

$$T_{M,2} = A_l \sin\left(\frac{2\pi P_0}{P_l} n + \phi_l\right) + T_0 + \Delta P_0 n \quad (2)$$

$$T_{M,3} = A_s \sin\left(\frac{2\pi P_0}{P_s} n + \phi_s\right) + T_0 + \Delta P_0 n + \frac{1}{2} P_0 \dot{P} n^2 + \dots \quad (3)$$

$$T_{M,4} = A_l \sin\left(\frac{2\pi P_0}{P_l} n + \phi_l\right) + A_s \sin\left(\frac{2\pi P_0}{P_s} n + \phi_s\right) + T_0 + \Delta P_0 n \quad (4)$$

where  $T_{M,N}$  is the model timing of the  $n$ th epoch of model  $N$ ;  $\dot{P}$  is the period time-derivative;  $\Delta P_0$  is a correction to the trial period  $P_0$ ; and  $A_{l/s}$ ,  $P_{l/s}$ , and  $\phi_{l/s}$  are the amplitude, period, and phase of the long/short-period sinusoidal components in models 2-4. All four models and their residuals are plotted in Fig. 3.

Models 1 and 3 involve a series expansion of the QPE period about  $P_0$ , carried out to quadratic order (a constant  $\dot{P}$ ). Models 2 and 4 consist only of sinusoidal modulation(s) of the burst arrival times, as is seen increasingly commonly in QPE timing analyses (Chakraborty et al. 2024a; Miniutti et al. 2025; Arcodia et al. in prep.). While the absolute values of  $\chi^2$  are meaningless given our ad hoc choice of a 0.1 d systematic error, the difference in reduced chi-squared can be used for qualitative model comparison. Models 1/2/3/4 have  $\chi^2/\text{dof.} = 14.9/15.9/2.9/3.1$  respectively. Models 3 and 4 are thus favored over 1 and 2, while model 3—a period derivative plus a short-term sinusoidal modulation—achieves the best fit statistic.

**Period derivative:** models 1 and 3 interpret the concave-up trend as a secular period increase expanded to quadratic order. The best-fitting model 1 corresponds to  $P_0 = 9.50 \pm 0.01$  d and  $\dot{P} = (1.67 \pm 0.01) \times 10^{-2}$  d d $^{-1}$  at  $T_0 = 60710.02 \pm 0.06$  MJD, whereas in model 3 it is  $P_0 = 9.48 \pm 0.02$  d and  $\dot{P} = (1.72 \pm 0.02) \times 10^{-2}$  d d $^{-1}$  at  $T_0 = 60710.10 \pm 0.09$  MJD.

**Long-period oscillation:** models 2 and 4 instead interpret the period increase as part of a long-term oscillation, and thus that the period will eventually decrease. This sinusoidal component in model 2 corresponds to an amplitude of  $A_l = 1872^{+2309}_{-1077}$  d with a period of  $P_l/P_0 = 681^{+338}_{-238}$  (or  $P_l \approx 17.7^{+8.8}_{-6.2}$  yr). In model

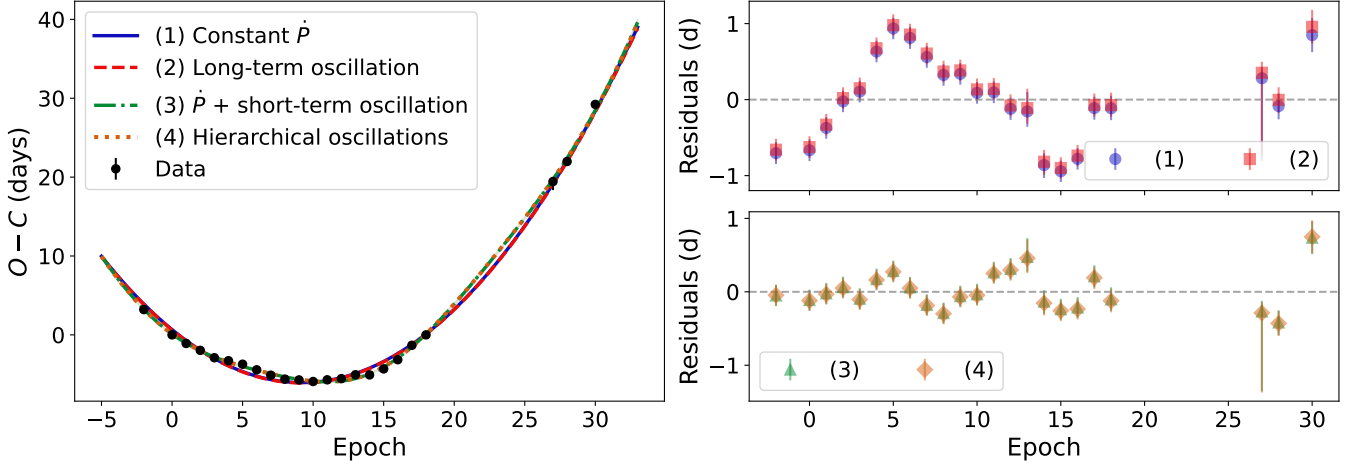


**Figure 3.** **Left:**  $O - C$  diagram of the QPEs overplotted with models 1-4. The data are consistent with  $P_0 \approx 9.5$  d and  $\dot{P} \approx 1.7 \times 10^{-2}$  d d $^{-1}$  at  $T_0 \approx 60710.1$ . In principle, it is possible that the apparent period increase is due to a long-term period oscillation observed locally (models 2 and 4); the  $> 1$  yr data baseline over which  $\dot{P}$  is constant constrains any such oscillation to have a period  $\gtrsim 11$  yr and amplitude  $\gtrsim 1000$  d. **Right:** data–model residuals. Models 1-2 show structured residuals, which models 3-4 interpret as a sine with period  $\sim 155$  d and amplitude  $\sim 0.8$  d (though see Appendix A).

4, the amplitude is  $A_l = 3068^{+1498}_{-1205}$  d with a period of  $P_l/P_0 = 863 \pm 190$  (or  $P_l \approx 22.4 \pm 4.9$  yr).

**Short-period oscillation:** motivated by the apparent sine-like residuals in models 1-2, models 3 and 4 contain an additional short-term modulation. In model 3 it has an amplitude of  $A_s = 0.79 \pm 0.05$  d and  $P_s/P_0 = 16.2 \pm 0.5$  (or  $P_s \approx 154$  d). In model 4 the amplitude is  $A_s = 0.79 \pm 0.05$  d, with period  $P_s/P_0 = 16.3 \pm 0.6$  (or  $P_s \approx 155$  d).

In summary, the data are consistent with a constant period derivative with  $P_0 \approx 9.5 \pm 0.02$  d and  $\dot{P} \approx (1.7 \pm 0.02) \times 10^{-2}$  d d $^{-1}$  at  $T_0 \approx 60710.1$ . This can instead be interpreted as a long-term period oscillation, in which case the period is  $\approx 11 - 27$  yr and the amplitude is  $\approx 1000 - 4500$  d. We also fit an additional shorter-period oscillation with  $A_s = 0.79 \pm 0.05$  d and period  $\approx 155$  d, though we caution that the 19 consecutive epochs span only  $\sim 1.2$  cycles, and that the reality of this secondary oscillation depends on the physical interpretation of the QPE-generating process (Appendix A).

We also note that the 2024 data showed recurrence times between  $\sim 4.5 - 7$  days (Fig. 1; Hernández-García et al. 2025a), which is considerably shorter than the  $P_0$  inferred from the 2025 data. However, given the long observation gap between 2024 and 2025, it is impossible to unambiguously assign epoch numbers to the 2024 data, so we cannot include them in the  $O - C$  analysis. Still, extrapolating the period backwards finds recurrence times plausibly consistent with the 2024 observations at epochs  $\lesssim -20$  (Fig. 4), providing a convenient explanation for those data. The inset panel of Fig. 4 extrapolates the period forwards, finding that the constant

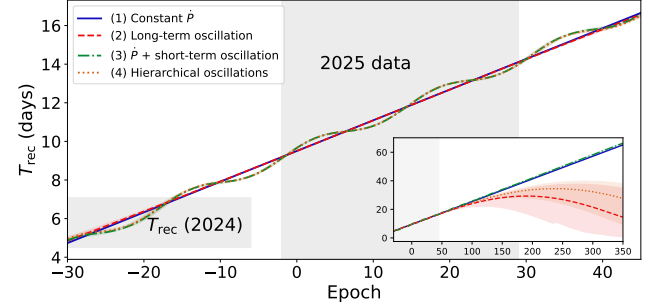


**Figure 4.** We plot the period evolution for the four  $O - C$  models. Shaded regions denote the 2025 data (Epochs -2–29) and the range of periods observed in 2024. The inset panel extrapolates over  $\sim$ few hundred epochs, showing the constant  $\dot{P}$  and long-term oscillation models begin to diverge after  $\gtrsim 100$  epochs.

$\dot{P}$  and long-term oscillation models begin to diverge at epochs  $\gtrsim 100$ .

#### 4. DISCUSSION

Given the ambiguity between a constant  $\dot{P} \approx 1.7 \times 10^{-2}$  d d $^{-1}$  or a long-term period oscillation over 11–27 yr, as well as the variety of physical processes which may be relevant to period evolution in repeating nuclear transients (Linial & Quataert 2024), we consider several models for the observed period change. In Sections 4.1–4.2 we assume QPEs are powered by repeatedly stripping mass from a bound star near pericenter (akin to a repeating TDE, though not necessarily accretion-powered), which results in a steady increase of the orbital period as in models 1 & 3. In Sections 4.3–4.4 we assume there is no secular change to the orbital pe-

riod, but that the apparent  $\dot{P}$  is the result of geometric light travel-time delays induced by general relativistic precession or the effect of a third body, à la models 2 & 4. Section 4.5 discusses the ability of disk instability models to describe the data.

#### 4.1. Orbital evolution due to mass-transfer

Mass transfer from a lower-mass donor to a larger-mass companion can counteract angular momentum-loss mechanisms such as gravitational-wave emission or tidal dissipation and cause binary orbits to expand, an effect which has even been known theoretically for decades (see e.g. Eggleton 2006) and even measured directly in a few ultracompact binary systems via eclipse timing (de Miguel et al. 2018; Chakraborty et al. 2024b). This result has been extended to eccentric mass-transferring stellar binaries by deriving equations for the time evolution of the osculating orbital elements, e.g. via the orbit-averaged Lagrange planetary equations under a perturbing force due to mass-transfer (Hadjidemetriou 1963; Sepinsky et al. 2009; Dosopoulou & Kalogera 2016a,b). While the general case depends on the orbital angular momentum retention factor, size of the donor’s Roche lobe, donor/accretor masses, and other uncertain system properties, most of these are linear-order in the mass ratio  $q \equiv M_*/M_\bullet$ , and can thus be dropped due to the extreme mass ratio in our system ( $q \sim 10^{-6}$ ). We follow Eqns. 43-44 of Dosopoulou & Kalogera (2016b), which assume delta-function Roche lobe overflow at pericenter and non-conservative mass transfer ( $\dot{M}_{\text{tot}}, \dot{J}_{\text{orb}} \neq 0$ ). In the EMRI approximation, the fractional change in orbital period ( $P_{\text{orb}}$ ) is then:

$$\frac{\Delta P_{\text{orb}}}{P_{\text{orb}}} \approx 3\zeta \left( \frac{\Delta M_*}{M_*} \right) \sqrt{1 - e^2} \quad (5)$$

where  $e$  is the orbital eccentricity;  $\Delta M_*$  is the fraction of the stellar mass loss per passage; and  $\zeta$  is the fraction of stripped mass captured by the primary, defined such that  $\Delta M_\bullet = -\zeta \Delta M_*$ , as opposed to being lost to infinity and carrying orbital angular momentum away with it (e.g. as in Linial & Sari 2017). We note that Eq. 5 is reminiscent of the Newtonian result of Hughes 2019 obtained by enforcing adiabatic invariance of the orbital actions assuming conservative mass-transfer. Though the methods differ, they found  $\Delta P_{\text{orb}}/P_{\text{orb}} = 3(\Delta M_*/M_*)$ ; our result differs by the order-unity factor  $\sqrt{1 - e^2}$  and the mass-retention term  $\zeta$ .

Similarly, the change in orbital eccentricity is:

$$\Delta e \approx 2\zeta \left( \frac{\Delta M_*}{M_*} \right) (1 - e) \sqrt{1 - e^2} \quad (6)$$

implying the eccentricity is excited to larger values as the semimajor axis increases. In Fig. 5 we plot the evo-

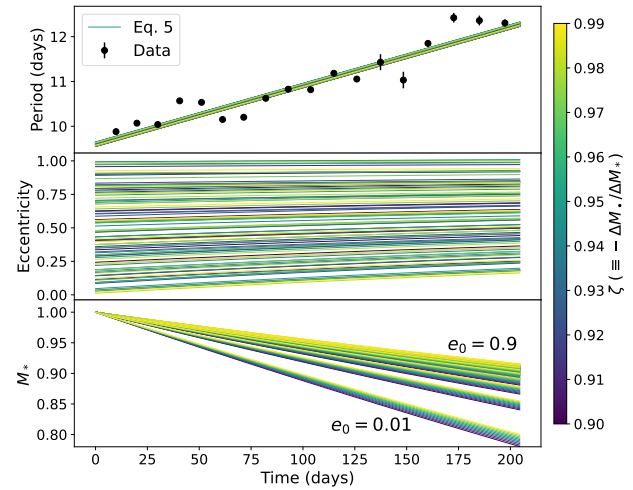


**Figure 5.** Evolution of  $P_{\text{orb}}$ ,  $e$ , and  $M_*$  for various choices of  $(e_0, \zeta)$ , assuming impulsive mass-loss occurs at pericenter, from Eqns. 5-6. Each trajectory on the top/middle panels has a random offset (up to 0.1/0.05 respectively) for visual clarity.

lution of  $P_{\text{orb}}$ ,  $M_*$ , and  $e$  according to Eqns. 5-6 for various choices of  $(e_0, \zeta)$ . The typical required fractional mass-loss per orbit is of order  $\Delta M_*/M_* \approx (4-8) \times 10^{-3}$ , increasing for lower initial eccentricities (as evident from Eq. 5). For a star of  $\sim M_\odot$ , this is a factor 10 – 1000 larger than estimated in Section 2 assuming a radiative efficiency of  $\eta \sim 0.01 - 1$ , but remarkably, is comparable to values found from the energetics of the time-evolving outflow reported in Ansley (Chakraborty et al. 2025b) implying  $\eta$  may be lower than previously assumed. The inferred fractional mass loss carries the dramatic implication that  $\sim 10\%$  of the stellar mass must be stripped within just a year, placing a strict bound on the continued eruption lifetime and predicting dramatic luminosity evolution should be seen in continued monitoring.

The assumption of mass-loss from the orbiting star places some constraints on its nature. The Roche lobe at pericenter is approximately:

$$R_L \approx 4.8R_\odot \left( \frac{P_{\text{orb}}}{11 \text{ d}} \right)^{2/3} \left( \frac{1 - e}{0.5} \right) \left( \frac{M_*}{M_\odot} \right)^{2/3} \quad (7)$$

meaning an orbiting companion with an outer radius of several  $\times R_\odot$  and/or  $e \gtrsim 0.9$  is required for Roche-lobe overflow. While assuming the main sequence mass-radius relation would imply this corresponds to a stellar mass of  $\sim 7M_\odot$ , recent work has found tidal heating in close proximity to the SMBH can lead to runaway radial expansion of the star (Yao & Quataert 2025), meaning even lower masses are plausible.

Dividing Eq. 5 by Eq. 6 and integrating implies that  $r_p \equiv a(1 - e)$  is a constant as  $a$  and  $e$  increase. This provides a convenient potential explanation for why the eruption luminosity and integrated energy per flare do not change dramatically throughout 2025 (Fig. 1). One major uncertainty with this model is whether, after losing  $\sim 10\%$  of its mass within a year, the stellar structure would remain constant enough to power continued eruptions of comparable luminosity, even at a fixed pericenter distance. To this end, Bandopadhyay et al. (2025) found that stars with masses  $\gtrsim 1M_\odot$  become a factor of few *denser* following the rapid stripping of 1-10% their masses (see their Figs. 5, 6 & 8), providing a circumstantial explanation for the lack of significant burst luminosity evolution (Fig. 1).

Another uncertainty concerns the viscous timescale, which is approximately (Shakura & Sunyaev 1973):

$$t_{\text{visc}} \sim 58 \text{ days} \left( \frac{0.1}{\alpha} \right) \left( \frac{0.1}{H/R} \right)^2 \left( \frac{M_\bullet}{10^6 M_\odot} \right) \left( \frac{R}{100 R_g} \right)^{3/2} \quad (8)$$

In comparison, the 2025 eruptions have durations of just 3 days. It is not clear how to reconcile the small required radii  $\lesssim 14R_g$  (for an assumed  $\alpha = 0.1$  and  $H/R = 0.1$ ) with the pericenter radii of  $\sim$ hundreds  $R_g$  inferred from the orbital period and  $M_\bullet$ . If stellar mass-loss is driving the QPEs, the flares themselves can be accretion-powered only if  $\alpha$  or  $H/R$  are  $\gg 0.1$ . Alternatively, a separate mechanism, such as collisional shocks of the stripped mass with the ambient disk, may be relevant for the system (e.g. Lu & Quataert 2023).

#### 4.2. Velocity kicks from tidal interaction with the SMBH

The models of mass-transfer driven orbital evolution in Section 4.1 are generally invoked for stellar-mass binaries, and do not consider the effects of the SMBH tidal field on the companion star. To this end, hydrodynamical simulations first carried out in Manukian et al. (2013) found the surprising result that, in contradiction to the expectations from linear tidal theory, partially disrupted stars around SMBHs can receive kicks which eject them on progressively more *unbound* orbits. This result was confirmed and extended by follow-up studies (Gaftron et al. 2015; Cufari et al. 2023; Chen et al. 2024), which generally attribute the positive-energy kicks to greater mass loss through L1 than L2. As mass flowing through L1 has a smaller orbital energy than the star, energy/momentum conservation can endow the stellar remnant with a positive-energy kick during its pericenter passage. This effect competes with deposition of orbital energy into tidal oscillatory modes of the star, which should decay the orbit; in general either may dom-

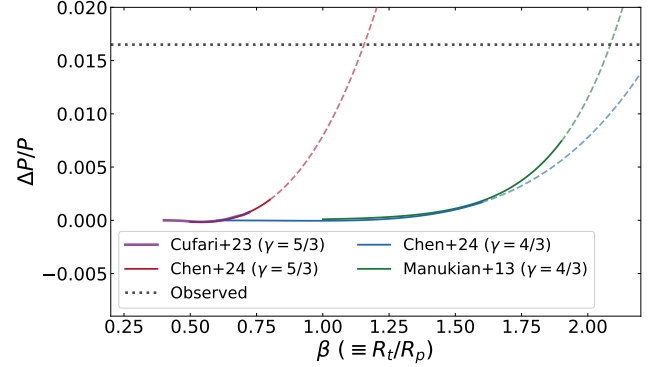


**Figure 6.** Magnitude of  $\Delta P_{\text{orb}}/P_{\text{orb}}$  resulting from velocity kicks to the partial TDE remnant, as a function of the penetration factor from various prior works. The dashed lines indicate extrapolations beyond the simulation results of the respective studies.

inate, resulting in different signs of  $\dot{P}$  in various regions of parameter space (Ryu et al. 2020; Chen et al. 2024). We also note that asymmetric mass loss is not definitively known to be the primary cause for this effect; see e.g. Coughlin & Nixon (2025) who propose an alternative mechanism related to the reformation of the stellar core after pericenter passage.

Manukian et al. (2013), Gaftron et al. (2015), and Chen et al. (2024) found partial disruptions can impart velocity kicks up to  $v_{\text{kick}} \lesssim v_{\text{esc}}$ , the escape speed of the orbiting star ( $= \sqrt{2GM_*/R_*}$ ), while Coughlin & Nixon (2025) found  $v_{\text{kick}}$  can even exceed  $v_{\text{esc}}$ . We relate an instantaneous kick velocity to a change in the specific orbital energy via  $v_{\text{kick}} = \sqrt{2\Delta\epsilon_{\text{kick}}}$ , following which the orbital period increases according to  $\Delta P_{\text{orb}}/P_{\text{orb}} = (3/2)(\Delta a/a) = (3/2)(\Delta\epsilon/\epsilon)$ . This can be cast in terms of  $v_{\text{kick}}/v_{\text{esc}}$  as:

$$\frac{\Delta P_{\text{orb}}}{P_{\text{orb}}} \approx 6 \times 10^{-3} \left( \frac{v_{\text{kick}}}{v_{\text{esc}}} \right)^2 \left( \frac{M_*}{M_\odot} \right) \left( \frac{R_*}{R_\odot} \right)^{-1} \times \left( \frac{M_\bullet}{10^6 M_\odot} \right)^{-2/3} \left( \frac{P_{\text{orb}}}{11 \text{ d}} \right)^{2/3} \quad (9)$$

implying main sequence stars require  $v_{\text{kick}} \gtrsim v_{\text{esc}}$  to attain the large  $\dot{P} \sim 10^{-2}$  observed in Ansley.

This is difficult to reconcile with the finding that larger kicks occur for more deeply-plunging orbits (larger  $\beta \equiv R_t/R_p$ ; e.g. Figure 7 of Gaftron et al. 2015). It is generally found that for  $\beta \lesssim 0.62$  the orbit shrinks, and only for  $\beta \gtrsim 0.62$  can the velocity kick outweigh tidal dissipation to expand the orbit (see e.g. Figure 1 of Cufari et al. 2023 and Figure 4 of Chen et al. 2024). In Fig. 6, we show the fractional change in orbital period resulting from pericenter kicks as a function of  $\beta$  resulting from several of these studies. We used the empiri-

ical fits of  $\Delta\epsilon_{\text{orb}}(\beta)$  provided in Eq. 9 of [Chen et al. \(2024\)](#) and  $v_{\text{kick}}/v_{\text{esc}}(\beta)$  in Fig. 3 of [Manukian et al. \(2013\)](#). The large magnitude of  $\dot{P}$  is only attained for near-complete disruptions ( $\beta \approx 1$  for  $\gamma = 5/3$  and  $\beta \approx 2$  for  $\gamma = 4/3$ ), at which point  $> 20$  consecutive eruptions of near-constant luminosity become impossible to explain. It is thus unlikely that kicks resulting from tidal interactions can explain the period change.

One remaining possibility may be a change not in the orbital period itself, but the return time of the debris after successive pericenter passages. See for instance [Bandopadhyay et al. \(2024\)](#), who found the peak fallback time scales with the angular velocity of the stellar core ( $\Omega$ ) as  $(1 + 2\Omega/\sqrt{GM_{\bullet}/r_p^3})^{0.8}$ . A thorough investigation of this idea is beyond the scope of this work.

### 4.3. General relativistic precession

Given the relatively constant burst energetics through 2025, it is worth considering whether the observed  $\dot{P}$  may be caused by an oscillatory change to the system geometry and/or light travel time due to relativistic precession(s), rather than a true change to the orbital semimajor axis. These are expected to induce measurable effects on QPE timings (e.g. [Xian et al. 2021](#); [Linial & Metzger 2023, 2024](#); [Franchini et al. 2023](#); [Zhou et al. 2024](#)), and such variations have already been observed in some cases ([Chakraborty et al. 2024a](#); [Miniutti et al. 2025](#); [Arcodia et al. in prep.](#)). Models 2 and 4 of Section 3 found a long-term precession period of 400–1050 epochs (11–27 yr) and an amplitude of 1000–4500 days; we consider whether the values can be reproduced.

The simplest relativistic effect is Schwarzschild (apsidal) precession. In this case, one would observe a sinusoidal period modulation due to light travel delays over the apsidal precession timescale ( $T_{\text{aps}}$ ), which is approximately  $T_{\text{aps}}/P_{\text{orb}} \approx a(1 - e^2)/(3R_g)$ . The semimajor axis is not known precisely due to uncertainty in  $M_{\bullet}$ , but  $a$  has a characteristic value:

$$a = 980R_g \left( \frac{P_{\text{orb}}}{11 \text{ d}} \right)^{2/3} \left( \frac{M_{\bullet}}{10^6 M_{\odot}} \right)^{-2/3} \quad (10)$$

meaning apsidal precession occurs over a timescale:

$$T_{\text{aps}} \approx 9.8 \text{ yr} (1 - e^2) \left( \frac{P_{\text{orb}}}{11 \text{ d}} \right)^{5/3} \left( \frac{M_{\bullet}}{10^6 M_{\odot}} \right)^{-2/3} \quad (11)$$

Let  $P_r$  be the radial period between successive pericenter passages, such that the  $n$ th passage is observed at:

$$t_n \approx nP_{\text{orb}} + \frac{r_p}{c} \cos \left( \frac{2\pi n P_{\text{orb}}}{T_{\text{aps}}} \right) \quad (12)$$

where we have assumed that the emission is generated close to  $r_p$ . The period measured by a distant observer

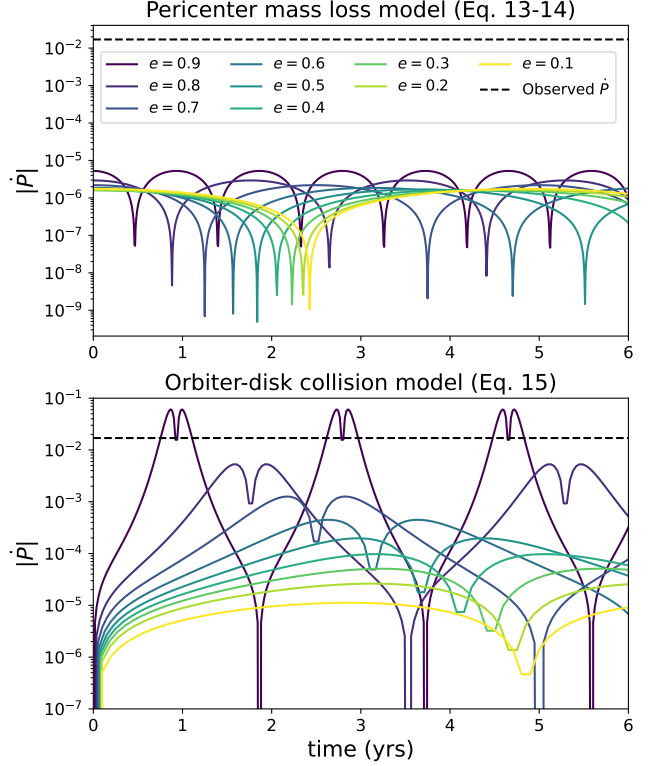


**Figure 7.**  $|\dot{P}|$  for two general relativistic precession models, with fiducial values  $M_{\bullet} = 10^6 M_{\odot}$  and  $P_{\text{orb}} = 11$  days. **Top:** model assuming QPE timings are set by pericenter passages (Eq. 13-14). **Bottom:** model assuming timings are set by orbiter-disk collisions (Eq. 15; [Linial & Quataert 2024](#)).

is  $P = dt_n/dn$ , so that the apparent  $dP/dt$  is:

$$\dot{P} = \frac{d^2 t_n}{dn^2} \frac{dn}{dt} = -\frac{4\pi^2 r_p P_{\text{orb}}}{c T_{\text{aps}}^2} \cos \left( \frac{2\pi n P_{\text{orb}}}{T_{\text{aps}}} \right) \quad (13)$$

where  $dn/dt = 1/P_{\text{orb}}$ . The maximum apparent period change resulting from this expression is:

$$\dot{P}_{\text{max}} \approx 1.9 \times 10^{-6} \frac{1 - e}{(1 - e^2)^2} \left( \frac{P_{\text{orb}}}{11 \text{ d}} \right)^{-5/3} \left( \frac{M_{\bullet}}{10^6 M_{\odot}} \right)^{5/3} \quad (14)$$

which is four orders of magnitude too small (unless  $e \rightarrow 1$ ). We plot  $|\dot{P}|$  for some choices of  $e$  in the top panel of Fig. 7.

We also consider the  $\dot{P}$  in a model where the QPEs arise from star-disk collisions rather than pericenter mass-loss. In this case, the impact timings change as the orbiter and disk precess, so  $\dot{P}$  reflects a true change in the system geometry, not just a light travel-time effect. The period derivative in this scenario was considered in Section 5.2, Eq. 40 of [Linial & Quataert \(2024\)](#):

$$\dot{P} \approx 10^{-4} \frac{e \sin \theta}{(1 - e^2)(1 + e \cos \theta)^3} \left( \frac{P_{\text{orb}}}{11 \text{ d}} \right)^{-4/3} \left( \frac{M_{\bullet}}{10^6 M_{\odot}} \right)^{4/3} \quad (15)$$

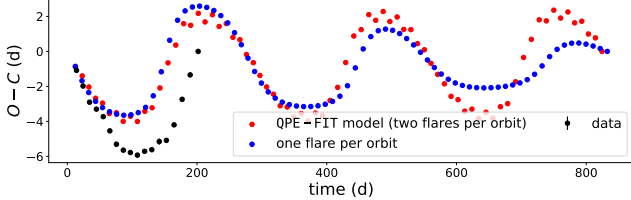


**Figure 8.**  $O - C$  diagrams of data (black) and maximum-likelihood QPE-FIT models assuming two (red) or one (blue) flares are produced per orbit.

For all but the most eccentric orbits, it remains difficult to produce the observed  $\dot{P} \sim 10^{-2}$  (Fig. 7 bottom). Even then, high- $e$  orbits maintain a large  $\dot{P}$  only for a brief period of  $\lesssim$ few months due to their short  $T_{\text{aps}}$ .

Further super-orbital variations, with longer timescales and larger amplitude, can occur due to Lense-Thirring (nodal) precession of the orbiter and/or the accretion disk (e.g. Franchini et al. 2023). While this is more difficult to model analytically, the effect can be readily simulated with the open-source EMRI/disk trajectory modeling code QPE-FIT<sup>1</sup> (Chakraborty et al. 2025c), which performs Bayesian inference using QPE timings to infer EMRI/disk parameters while including relativistic precession of the orbiter and disk. We show the best-fitting models in Fig. 8: though the modulation amplitude can be approximately reproduced, the long modulation timescale cannot be captured simultaneously. This is the same tension we saw in Eq. 15: large-amplitude geometric delays require highly eccentric orbits, but larger  $e$  shortens the precession timescales compared to the year baseline over which we observe a stable  $\dot{P}$ .

It is worth noting the *short*-period oscillation in  $O - C$  models 3-4, with  $P_s \approx 155$  d and amplitude 0.8 d, is plausibly consistent with relativistic precession. A 155 d period requires  $e \gtrsim 0.97$  (Eq. 11)—which is not impossible (e.g. the orbit of S2 around Sgr A\*)—and the amplitude  $\ll T_{\text{rec}}$  is significantly easier to obtain.

In any case, from the above arguments and the  $O - C$  constraints it appears unlikely that the apparent  $\dot{P}$  is entirely the result of relativistic precession, due to the long modulation timescales (11 – 27 yr) and amplitudes (1000 – 4500 days). It is possible that a large SMBH mass  $\gg 10^6 M_{\odot}$  may increase the variation amplitude (e.g. Eq. 15), but this would both decrease the precession period (Eq. 11) and be in tension with host galaxy scaling relation-based estimates of  $M_{\bullet}$  (Sánchez-Sáez et al. 2024; Zhu et al. 2025). It may thus be that reproducing the data requires a previously unconsidered source

of precession-induced timing variation—an increasingly common conclusion of QPE timing studies (Minutti et al. 2025; Arcodia et al. in prep.). While the most direct confirmation of this model would be eventually measuring the change to  $\dot{P}$  predicted by long-term precession after a few years (Fig. 5), this may be achieved earlier by directly measuring  $\ddot{P}$ .

#### 4.4. Hierarchical SMBH binary

Another possibility is the presence of an outer SMBH which induces the apparent period change via geometric light travel-time delays due to reflex motion of the QPE-emitting system, a situation comparable to models 2 and 4 of Section 3 (see also Minutti et al. 2025). An SMBH binary with period  $P_{\text{SMBH}}$ , orbital velocity  $v_{\text{orb}}$ , and frequency  $\omega_{\text{orb}}$  would induce an apparent  $\dot{P} = (P\omega_{\text{orb}}v_{\text{orb}}/c) \cos(\omega_{\text{orb}}t)$  for an edge-on observer. For an equal-mass circular binary, the maximum apparent derivative for an edge-on observer is then:

$$\dot{P}_{\text{max}} \approx 4.4 \times 10^{-5} \left( \frac{M_{\text{tot}}}{2 \times 10^6 M_{\odot}} \right)^{1/3} \left( \frac{P_{\text{SMBH}}}{20 \text{ yr}} \right)^{-4/3} \left( \frac{P}{11 \text{ d}} \right) \quad (16)$$

with  $\dot{P}$  decreased by  $\sin \theta$  for smaller viewing angles. An SMBH binary thus cannot account for the period change due to our simultaneous constraints on the large magnitude of  $\dot{P}$  and the long oscillation timescale ( $\gtrsim 11$  yr).

#### 4.5. Disk instability model

Prior work has also explored the applicability of disk instability models for QPEs (e.g. Śniegowska et al. 2020; Pan et al. 2022). As in the standard Shakura & Sunyaev (1973) treatment, they find that SMBH accretion disks of sufficiently high Eddington ratio ( $\dot{m} \equiv \dot{M}/\dot{M}_{\text{Edd}} \gtrsim 0.01$ ) are thermally and viscously unstable in the inner radiation pressure-dominated region. These disks are known to undergo limit cycles, whereby material gradually accumulates, then rapidly accretes onto the black hole in recurrent outbursts. While this normally occurs on the viscous timescale, for narrow unstable regions—of width  $\Delta R$  at radius  $R$ —the timescale can be reduced by order  $\Delta R/R$  (Śniegowska et al. 2020). Pan et al. (2022) proposed that large-scale poloidal magnetic fields can confine the unstable region to  $\Delta R \sim 0.1 R_S$  by driving winds to remove angular momentum and cool the disk; QPEs are then driven by limit cycles in this inner ring rather than the entire disk, producing qualitative agreement with the timescales and energetics of most QPEs (Pan et al. 2023).

Pan et al. (2025) subsequently found that burst recurrence times may vary by factors of several, even for

<sup>1</sup> <https://github.com/joheenc/QPE-FIT>

percent-level changes in  $\dot{m}$ . They identified a critical threshold near  $\dot{m}_{\text{crit}} \approx 0.1$ , dependent on the magnetic field strength, below which  $T_{\text{rec}}$  remains relatively stable and above which the sensitivity of  $T_{\text{rec}}$  to  $\dot{m}$  increases dramatically (see their Figure 1). It is thus possible that, if  $\dot{m}$  increased from  $\lesssim \dot{m}_{\text{crit}}$  in 2024 to  $\gtrsim \dot{m}_{\text{crit}}$  in 2025, and is now increasing steadily, the observed period evolution in Ans sky could be produced. Only a modest long-term increase in  $\dot{m}$  would be required, and such a trend has already been observed in other QPEs (e.g. Miniutti et al. 2023).

There are some immediate uncertainties in this picture. Ans sky's quiescence emission was detected in three *XMM-Newton* observations: OBSID 0935191501 in July 2024 (presented in Hernández-García et al. 2025a), and OBSIDs 096450101 and 096450301 in July 2025. Assuming a multicolor disk blackbody model for both epochs, we estimated 0.3-2 keV luminosities of  $L_{q,2024} = (4.1 \pm 1.2) \times 10^{40}$  and  $L_{q,2025} = (2.9 \pm 0.3) \times 10^{40}$  erg s $^{-1}$ , respectively, i.e. a constant luminosity within errors. The steady-state accretion rate is then:

$$\dot{m} \approx 0.03 \left( \frac{L_{X,\text{quiesc}}}{3 \times 10^{40} \text{erg s}^{-1}} \right) \left( \frac{\eta_X}{100} \right) \left( \frac{M_{\bullet}}{10^6 M_{\odot}} \right) \quad (17)$$

where  $\eta_X \equiv L_{\text{bol}}/L_X$  is the bolometric correction factor. Achieving  $\dot{m}_{\text{crit}} \approx 0.1$  would require  $\eta_X \gtrsim 300$ , a factor of a 3 – 30 larger than typical for TDE disks (e.g. Mummery et al. 2023). While this is not impossible given uncertainties in  $M_{\bullet}$ ,  $\eta_X$ , and  $\dot{m}_{\text{crit}}$ , further work is needed to determine whether these tensions present an existential problem for the disk instability model.

## 5. CONCLUSION

We reported the surprising result that the quasi-period eruptions (QPEs) in ZTF19acnskyy/“Ans sky” have shown a smoothly *increasing* period throughout 2025-2026, consistent with a time-derivative  $\dot{P} \approx (1.7 \pm 0.02) \times 10^{-2}$  (Fig. 3). Backwards-extrapolating the  $\dot{P}$  implies that the 4.5 – 7 day recurrence times observed in 2024 data are expected  $\gtrsim 20$  QPEs before those in 2025, providing a partial explanation for the previous data. The period derivative has remained constant for over a full year thus far, ruling out period oscillations with  $P \lesssim 11$  yr or amplitude  $\lesssim 1000$  d. It remains possible that a very long-term sinusoidal modulation, of period  $\sim 11 - 27$  yr and amplitude  $\sim 1000 - 4500$  d, is responsible for the observed period increase, though that is about equally challenging to explain.

We considered several physical models for the period derivative, all of which face shortcomings:

1. Prior work has calculated the orbital evolution due to pericenter mass-transfer in eccentric stellar-

mass binaries via the orbit-averaged Lagrange planetary equations (e.g. Sepinsky et al. 2009; Dosopoulou & Kalogera 2016b). Extending these results to EMRIs, the observed  $\dot{P}$  can be reproduced for fractional mass losses of  $\Delta M_* \sim 10^{-3} M_*$  per passage (Eq. 5), even for non-conservative mass-transfer ( $M_{\text{tot}}, \dot{J}_{\text{orb}} \neq 0$ ). Two uncertainties are whether the stellar structure can sustain many consecutive comparable-energy bursts after losing  $\sim 10\%$  of its mass over a year (Fig. 5), and whether the  $\sim 58$  day viscous time at pericenter can be reconciled with the  $\lesssim 3$ -day burst duration.

2. Hydrodynamical simulations of partial TDEs have found that for large penetration factors, the remnants can receive a positive-energy kicks from asymmetric mass-loss and/or the reformation of the core, making their orbit progressively unbound (Manukian et al. 2013; Gafton et al. 2015; Cufari et al. 2023; Chen et al. 2024; Coughlin & Nixon 2025). The observed magnitude of  $\dot{P}$  would require  $v_{\text{kick}} \gtrsim v_{\text{esc}}$  (Eq. 9), which can be obtained for relatively deeply-plunging orbits ( $R_p \approx R_t$ ). However, this is impossible to reconcile with the energetics across  $> 30$  eruptions.
3. We also examined whether the period changes may be produced by general relativistic precession. We considered the effects of apsidal motion (Eqns. 13–15; Linial & Quataert 2024) and nodal precession of the orbiter/accretion disk (Franchini et al. 2023; Chakraborty et al. 2025c), finding the large  $\dot{P}$  amplitude and the long duration over which it is stable are difficult to reproduce simultaneously (Figs. 7–8). Given that no known combination of relativistic precessions appears readily able to explain the data, models for precession-induced timing variations may require extension, a theme also seen in other recent QPE timing studies (Miniutti et al. 2025; Arcodia et al. in prep.).
4. In a similar vein, we considered whether an outer SMBH binary can produce an apparent period change due to light travel-time delays induced by the reflex motion of the QPE-emitting system, and found the inferred  $\dot{P}$  falls short by  $\sim 3$  orders of magnitude.
5. Disk instability models invoking radiation pressure-driven limit cycles in a magnetically-confined ring near the ISCO (e.g. Śniegowska et al. 2020; Pan et al. 2022) appear qualitatively able to reproduce both the relatively steady 4.5 – 7 day recurrence times in 2024 and the smooth increase

in 2025, if the accretion rate steadily increases by a few percent (Pan et al. 2025). However, the measured quiescence X-ray luminosity and recurrence timescales are not immediately compatible with the numerical ranges explored in the literature, motivating further work. Moreover, it remains unclear what physical process can set such a stable underlying clock in the disk instability picture.

Most of the models predict an eventual change to the QPE properties. Scenarios involving a secular increase to the EMRI orbital radius require large stellar mass loss to drive the dramatic period change, implying both that the burst luminosities should change as the stellar structure responds, and that the QPEs should have a finite duration of  $\lesssim$  years. The relativistic precession model clearly predicts that eventually  $\dot{P}$  should decrease in magnitude, then change sign, though the constraints already placed from the long-term stability of  $\dot{P}$  mean this would only be observable after at least a few years (Fig. 5). Continued monitoring of the burst timings and energetics, and continued refinement of physical models

for QPEs, are thus well-motivated as the remarkable diversity of unexpected QPE phenomenology only grows.

## ACKNOWLEDGEMENTS

We thank Keith Gendreau, Zaven Arzoumanian, Scott Hughes, Eric Coughlin, Xin Pan, Daniel D’Orazio, Hengxiao Guo, and Zhen Yan for discussions and data which contributed to this work. We are particularly grateful to the *NICER* team for providing an exceptionally high-quality dataset which uniquely enabled this analysis. GM acknowledges support from grant n. PID2023-147338NB-C21 funded by Spanish MICIU/AEI/10.13039/501100011033 and ERDF/EU. JC acknowledges financial support from ANID – FONDECYT Regular 1251444, and Millennium Science Initiative Program NCN2023\_002. LHG acknowledges financial support from ANID program FONDECYT Iniciación 11241477. MG is funded by Spanish MICIU/AEI/10.13039/501100011033 and ERDF/EU grant PID2023-147338NB-C21.

## REFERENCES

Arcodia, R., Merloni, A., Nandra, K., et al. 2021, *Nature*, 592, 704, doi: [10.1038/s41586-021-03394-6](https://doi.org/10.1038/s41586-021-03394-6)

Arcodia, R., Miniutti, G., Ponti, G., et al. 2022, *A&A*, 662, A49, doi: [10.1051/0004-6361/202243259](https://doi.org/10.1051/0004-6361/202243259)

Arcodia, R., Liu, Z., Merloni, A., et al. 2024, *A&A*, 684, A64, doi: [10.1051/0004-6361/202348881](https://doi.org/10.1051/0004-6361/202348881)

Arcodia, R., Baldini, P., Merloni, A., et al. 2025, *ApJ*, 989, 13, doi: [10.3847/1538-4357/adec9b](https://doi.org/10.3847/1538-4357/adec9b)

Arcodia et al. in prep.

Baldini, P., Rau, A., Merloni, A., et al. 2026, arXiv e-prints, arXiv:2602.03932, doi: [10.48550/arXiv.2602.03932](https://doi.org/10.48550/arXiv.2602.03932)

Bandopadhyay, A., Coughlin, E. R., & Nixon, C. J. 2025, *ApJ*, 987, 16, doi: [10.3847/1538-4357/add9a5](https://doi.org/10.3847/1538-4357/add9a5)

Bandopadhyay, A., Coughlin, E. R., Nixon, C. J., & Pasham, D. R. 2024, *ApJ*, 974, 80, doi: [10.3847/1538-4357/ad6a5a](https://doi.org/10.3847/1538-4357/ad6a5a)

Cash, W. 1979, *ApJ*, 228, 939, doi: [10.1086/156922](https://doi.org/10.1086/156922)

Chakraborty, J., Kara, E., Masterson, M., et al. 2021, *ApJL*, 921, L40, doi: [10.3847/2041-8213/ac313b](https://doi.org/10.3847/2041-8213/ac313b)

Chakraborty, J., Arcodia, R., Kara, E., et al. 2024a, *ApJ*, 965, 12, doi: [10.3847/1538-4357/ad2941](https://doi.org/10.3847/1538-4357/ad2941)

Chakraborty, J., Burdge, K. B., Rappaport, S. A., et al. 2024b, *ApJ*, 977, 262, doi: [10.3847/1538-4357/ad9563](https://doi.org/10.3847/1538-4357/ad9563)

Chakraborty, J., Kara, E., Arcodia, R., et al. 2025a, *ApJL*, 983, L39, doi: [10.3847/2041-8213/adc2f8](https://doi.org/10.3847/2041-8213/adc2f8)

Chakraborty, J., Kosec, P., Kara, E., et al. 2025b, *ApJ*, 984, 124, doi: [10.3847/1538-4357/adb972](https://doi.org/10.3847/1538-4357/adb972)

Chakraborty, J., Drummond, L. V., Bonetti, M., et al. 2025c, *ApJ*, 992, 120, doi: [10.3847/1538-4357/ae003b](https://doi.org/10.3847/1538-4357/ae003b)

Chen, J.-H., Dai, L., Liu, S.-F., & Ou, J.-W. 2024, *ApJ*, 977, 80, doi: [10.3847/1538-4357/ad8b24](https://doi.org/10.3847/1538-4357/ad8b24)

Coughlin, E. R., & Nixon, C. J. 2025, *MNRAS*, 542, L110, doi: [10.1093/mnrasl/sla076](https://doi.org/10.1093/mnrasl/sla076)

Cufari, M., Nixon, C. J., & Coughlin, E. R. 2023, *MNRAS*, 520, L38, doi: [10.1093/mnrasl/slad001](https://doi.org/10.1093/mnrasl/slad001)

de Miguel, E., Patterson, J., Kemp, J., et al. 2018, *ApJ*, 852, 19, doi: [10.3847/1538-4357/aa9ed6](https://doi.org/10.3847/1538-4357/aa9ed6)

Dosopoulou, F., & Kalogera, V. 2016a, *ApJ*, 825, 70, doi: [10.3847/0004-637X/825/1/70](https://doi.org/10.3847/0004-637X/825/1/70)

—. 2016b, *ApJ*, 825, 71, doi: [10.3847/0004-637X/825/1/71](https://doi.org/10.3847/0004-637X/825/1/71)

Eggleton, P. 2006, *Evolutionary Processes in Binary and Multiple Stars*

Evans, P. A., Page, K. L., Beardmore, A. P., et al. 2023, *MNRAS*, 518, 174, doi: [10.1093/mnras/stac2937](https://doi.org/10.1093/mnras/stac2937)

Franchini, A., Bonetti, M., Lupi, A., et al. 2023, *A&A*, 675, A100, doi: [10.1051/0004-6361/202346565](https://doi.org/10.1051/0004-6361/202346565)

Gafton, E., Tejeda, E., Guillochon, J., Korobkin, O., & Rosswog, S. 2015, *MNRAS*, 449, 771, doi: [10.1093/mnras/stv350](https://doi.org/10.1093/mnras/stv350)

Gendreau, K. C., Arzoumanian, Z., Adkins, P. W., et al. 2016, in Society of Photo-Optical Instrumentation Engineers (SPIE) Conference Series, Vol. 9905, Space Telescopes and Instrumentation 2016: Ultraviolet to Gamma Ray, ed. J.-W. A. den Herder, T. Takahashi, & M. Bautz, 99051H, doi: [10.1117/12.2231304](https://doi.org/10.1117/12.2231304)

Giustini, M., Miniutti, G., & Saxton, R. D. 2020, *A&A*, 636, L2, doi: [10.1051/0004-6361/202037610](https://doi.org/10.1051/0004-6361/202037610)

Hadjidemetriou, J. D. 1963, *Icarus*, 2, 440, doi: [10.1016/0019-1035\(63\)90072-1](https://doi.org/10.1016/0019-1035(63)90072-1)

Hernández-García, L., Chakraborty, J., Sánchez-Sáez, P., et al. 2025a, *Nature Astronomy*, 9, 895, doi: [10.1038/s41550-025-02523-9](https://doi.org/10.1038/s41550-025-02523-9)

Hernández-García, L., Sánchez-Sáez, P., Chakraborty, J., et al. 2025b, *A&A*, 703, A263, doi: [10.1051/0004-6361/202555258](https://doi.org/10.1051/0004-6361/202555258)

Hughes, S. A. 2019, *PhRvD*, 100, 064001, doi: [10.1103/PhysRevD.100.064001](https://doi.org/10.1103/PhysRevD.100.064001)

Kaastra, J. S., & Bleeker, J. A. M. 2016, *A&A*, 587, A151, doi: [10.1051/0004-6361/201527395](https://doi.org/10.1051/0004-6361/201527395)

Kaur, K., Stone, N. C., & Gilbaum, S. 2023, *MNRAS*, 524, 1269, doi: [10.1093/mnras/stad1894](https://doi.org/10.1093/mnras/stad1894)

King, A. 2020, *MNRAS*, 493, L120, doi: [10.1093/mnrasl/slaa020](https://doi.org/10.1093/mnrasl/slaa020)

Koen, C. 2006, *MNRAS*, 365, 489, doi: [10.1111/j.1365-2966.2005.09719.x](https://doi.org/10.1111/j.1365-2966.2005.09719.x)

Krolik, J. H., & Linial, I. 2022, *ApJ*, 941, 24, doi: [10.3847/1538-4357/ac9eb6](https://doi.org/10.3847/1538-4357/ac9eb6)

Linial, I., & Metzger, B. D. 2023, *ApJ*, 957, 34, doi: [10.3847/1538-4357/acf65b](https://doi.org/10.3847/1538-4357/acf65b)

—. 2024, *ApJ*, 973, 101, doi: [10.3847/1538-4357/ad639e](https://doi.org/10.3847/1538-4357/ad639e)

Linial, I., Metzger, B. D., & Quataert, E. 2025, *ApJ*, 991, 147, doi: [10.3847/1538-4357/adfa0e](https://doi.org/10.3847/1538-4357/adfa0e)

Linial, I., & Quataert, E. 2024, *MNRAS*, 527, 4317, doi: [10.1093/mnras/stad3470](https://doi.org/10.1093/mnras/stad3470)

Linial, I., & Sari, R. 2017, *MNRAS*, 469, 2441, doi: [10.1093/mnras/stx1041](https://doi.org/10.1093/mnras/stx1041)

—. 2023, *ApJ*, 945, 86, doi: [10.3847/1538-4357/acbd3d](https://doi.org/10.3847/1538-4357/acbd3d)

Lu, W., & Quataert, E. 2023, *MNRAS*, 524, 6247, doi: [10.1093/mnras/stad2203](https://doi.org/10.1093/mnras/stad2203)

Manukian, H., Guillochon, J., Ramirez-Ruiz, E., & O’Leary, R. M. 2013, *ApJL*, 771, L28, doi: [10.1088/2041-8205/771/2/L28](https://doi.org/10.1088/2041-8205/771/2/L28)

Middleton, M., Gúrpide, A., Kwan, T. M., et al. 2025, *MNRAS*, 537, 1688, doi: [10.1093/mnras/staf052](https://doi.org/10.1093/mnras/staf052)

Miniutti, G., Giustini, M., Arcodia, R., et al. 2023, *A&A*, 670, A93, doi: [10.1051/0004-6361/202244512](https://doi.org/10.1051/0004-6361/202244512)

Miniutti, G., Saxton, R. D., Giustini, M., et al. 2019, *Nature*, 573, 381, doi: [10.1038/s41586-019-1556-x](https://doi.org/10.1038/s41586-019-1556-x)

Miniutti, G., Franchini, A., Bonetti, M., et al. 2025, *A&A*, 693, A179, doi: [10.1051/0004-6361/202452400](https://doi.org/10.1051/0004-6361/202452400)

Mummery, A. 2025, arXiv e-prints, arXiv:2504.21456, doi: [10.48550/arXiv.2504.21456](https://doi.org/10.48550/arXiv.2504.21456)

Mummery, A., Wevers, T., Saxton, R., & Pasham, D. 2023, *MNRAS*, 519, 5828, doi: [10.1093/mnras/stac3798](https://doi.org/10.1093/mnras/stac3798)

Nicholl, M., Pasham, D. R., Mummery, A., et al. 2024, *Nature*, 634, 804, doi: [10.1038/s41586-024-08023-6](https://doi.org/10.1038/s41586-024-08023-6)

Pan, X., Li, S.-L., & Cao, X. 2023, *ApJ*, 952, 32, doi: [10.3847/1538-4357/acd180](https://doi.org/10.3847/1538-4357/acd180)

Pan, X., Li, S.-L., Cao, X., Liu, B., & Yuan, W. 2025, *ApJ*, 989, 196, doi: [10.3847/1538-4357/adf05d](https://doi.org/10.3847/1538-4357/adf05d)

Pan, X., Li, S.-L., Cao, X., Miniutti, G., & Gu, M. 2022, *ApJL*, 928, L18, doi: [10.3847/2041-8213/ac5faf](https://doi.org/10.3847/2041-8213/ac5faf)

Quintin, E., Webb, N. A., Guillot, S., et al. 2023, *A&A*, 675, A152, doi: [10.1051/0004-6361/202346440](https://doi.org/10.1051/0004-6361/202346440)

Raj, A., & Nixon, C. J. 2021, *ApJ*, 909, 82, doi: [10.3847/1538-4357/abdc25](https://doi.org/10.3847/1538-4357/abdc25)

Ryu, T., Krolik, J., Piran, T., & Noble, S. C. 2020, *ApJ*, 904, 100, doi: [10.3847/1538-4357/abb3ce](https://doi.org/10.3847/1538-4357/abb3ce)

Sánchez-Sáez, P., Hernández-García, L., Bernal, S., et al. 2024, *A&A*, 688, A157, doi: [10.1051/0004-6361/202347957](https://doi.org/10.1051/0004-6361/202347957)

Sepinsky, J. F., Willems, B., Kalogera, V., & Rasio, F. A. 2009, *ApJ*, 702, 1387, doi: [10.1088/0004-637X/702/2/1387](https://doi.org/10.1088/0004-637X/702/2/1387)

Shakura, N. I., & Sunyaev, R. A. 1973, *A&A*, 24, 337

Śniegowska, M., Czerny, B., Bon, E., & Bon, N. 2020, *A&A*, 641, A167, doi: [10.1051/0004-6361/202038575](https://doi.org/10.1051/0004-6361/202038575)

Śniegowska, M., Grzędzierski, M., Czerny, B., & Janiuk, A. 2023, *A&A*, 672, A19, doi: [10.1051/0004-6361/202243828](https://doi.org/10.1051/0004-6361/202243828)

Suková, P., Zajaček, M., Witzany, V., & Karas, V. 2021, *ApJ*, 917, 43, doi: [10.3847/1538-4357/ac05c6](https://doi.org/10.3847/1538-4357/ac05c6)

Tagawa, H., & Haiman, Z. 2023, *MNRAS*, 526, 69, doi: [10.1093/mnras/stad2616](https://doi.org/10.1093/mnras/stad2616)

Vaughan, S., Uttley, P., Markowitz, A. G., et al. 2016, *MNRAS*, 461, 3145, doi: [10.1093/mnras/stw142](https://doi.org/10.1093/mnras/stw142)

Xian, J., Zhang, F., Dou, L., He, J., & Shu, X. 2021, *ApJL*, 921, L32, doi: [10.3847/2041-8213/ac31aa](https://doi.org/10.3847/2041-8213/ac31aa)

Yao, P. Z., & Quataert, E. 2025, arXiv e-prints, arXiv:2505.10611, doi: [10.48550/arXiv.2505.10611](https://doi.org/10.48550/arXiv.2505.10611)

Yao, P. Z., Quataert, E., Jiang, Y.-F., Lu, W., & White, C. J. 2025, *ApJ*, 978, 91, doi: [10.3847/1538-4357/ad8911](https://doi.org/10.3847/1538-4357/ad8911)

Zhou, C., Zhong, B., Zeng, Y., Huang, L., & Pan, Z. 2024, arXiv e-prints, arXiv:2405.06429, doi: [10.48550/arXiv.2405.06429](https://doi.org/10.48550/arXiv.2405.06429)

Zhu, J., Jiang, N., Wang, Y., et al. 2025, *ApJL*, 994, L16, doi: [10.3847/2041-8213/ae19ea](https://doi.org/10.3847/2041-8213/ae19ea)

## APPENDIX

A. ON THE INTERPRETATION OF RESIDUALS IN  $O - C$  CURVES

The interpretation of the  $O - C$  residuals depends on whether the processes generating QPE timings are governed by a deterministic underlying clock (e.g. a binary orbit) or not (e.g. an accretion instability). Suppose there is an underlying “noisy clock”, with mean period  $P_0$  and derivative  $\dot{P}$ , that exhibits uncorrelated random timing noise of characteristic size  $\Delta t$ . Then, the  $n$ th burst occurs at:

$$t_n = P_0 n + \frac{1}{2} P_0 \dot{P} n^2 + \Delta t_n \quad (\text{A1})$$

The  $O - C$  residuals after subtracting the deterministic model  $P_0 n + (1/2)P_0 \dot{P} n^2$  are:

$$(O - C)_{n, \text{clock}} = \Delta t_n \quad (\text{A2})$$

i.e. uncorrelated white noise. However, if no underlying clock exists, each burst timing depends on the previous one:

$$\begin{aligned} t_n &= t_{n-1} + P_0 + P_0 \dot{P} n + \Delta t_n \\ &\approx P_0 n + \frac{1}{2} P_0 \dot{P} n^2 + \sum_{m=1}^n \Delta t_m \end{aligned} \quad (\text{A3})$$

yielding cumulative residuals:

$$(O - C)_{n, \text{no clock}} = \sum_{m=1}^n \Delta t_m \quad (\text{A4})$$

which is a random walk with a red noise power spectrum  $\propto 1/f^2$ . The characteristic amplitude of a spurious sinusoidal signal over the full baseline is thus of order:

$$A_{\text{rms}} \approx \Delta t \sqrt{N} \quad (\text{A5})$$

For a sinusoid of period  $P_{\text{sin}} < N$ , the RMS displacement shrinks to  $\Delta t \sqrt{P_{\text{sin}}}$ , meaning the longest periods allowed by the observation—that is, the full baseline—are the most prone to the appearance of false sine-like residuals arising from random walk noise. In other words, when interpreting residuals of QPE timing  $O - C$  curves *without* the EMRI picture, one must account for the possibility that apparent periodicities of modest amplitudes and periods comparable to the observing baseline are driven by stochastic noise—an insight all too familiar in the contexts of of accretion variability (Vaughan et al. 2016) and even binary eclipse timing (Koen 2006).

Consider the two  $O - C$  components identified in Section 3. Prior to including the period derivative term, the  $O - C$  curve reaches a maximum of  $\sim 30$  days over 33 epochs (Fig. 3). Explaining this via random noise requires  $\Delta t \sim 5.3$  d (Eq. A5). Compared to the underlying periodicity of  $\sim 11$  d, this demands a clock unstable at nearly the 50% level. This is certainly unreasonable for any orbital phenomenon; while such a statement cannot be made definitively in the disk instability model, it is nevertheless an extreme variation. The physical reality of the  $\dot{P}$  term is thus almost model-independent.

On the other hand, for the short-period oscillation with  $A_s = 0.8$  d, Eq. A5 gives  $\Delta t \sim 0.14$  d, only  $\sim 1\%$  of the QPE recurrence time. The deterministic orbital model predicts white noise in the  $O - C$  residuals, so a sine term to capture the additional structure is well-justified even for the small amplitude (i.e. models 3-4 of Section 3). However, disk instability models could easily produce red noise at this level; if the true QPE-generating process is not orbital, then models 3-4 are not necessary. While it is a subtle point, the necessity of additional terms to capture structured residuals in the  $O - C$  curve depends on the physical interpretation of what one believes is actually driving the QPEs.